remote sensing

MDPI

Article

Sea Level Budget in the East China Sea Inferred from Satellite Gravimetry, Altimetry and Steric Datasets

Fengwei Wang [1,2], Jianhua Geng [2,3,*], Yunzhong Shen [1], Jianli Chen [4,5], Anny Cazenave [6], Qiujie Chen [1], Le Chang [7] and Wei Wang [1]

[1] College of Surveying and Geo-Informatics, Tongji University, Shanghai 200092, China; wangfw-foster@tongji.edu.cn (F.W.); yzshen@tongji.edu.cn (Y.S.); qiujiechen@tongji.edu.cn (Q.C.); wangwei_96@tongji.edu.cn (W.W.)
[2] State Key Laboratory of Marine Geology, Tongji University, Shanghai 200092, China
[3] School of Ocean and Earth Science, Tongji University, Shanghai 200092, China
[4] Department of Land Surveying and Geo-Informatics, The Hong Kong Polytechnic University, Hong Kong 999077, China; jianli.chen@polyu.edu.hk
[5] Research Institute for Land and Space, The Hong Kong Polytechnic University, Hong Kong 999077, China
[6] Laboratoire d'Etudes en Géophysique et Océanographie Spatiales, 31400 Toulouse, France; anny.cazenave@issibern.ch
[7] College of Geomatics, Xi'an University of Science and Technology, Xi'an 710054, China; changle114@mails.ucas.edu.cn
* Correspondence: jhgeng@tongji.edu.cn

Abstract: The regional sea level budget in the East China Sea (ECS) was investigated with satellite gravimetry, altimetry, steric and sediment datasets over the period from April 2002 to December 2022. The "sediment effect" due to the difference between the change in sediment mass and the displaced original seawater should be removed from the total mass change observed by satellite gravimetry data to accurately estimate the manometric sea level change associated with the variations in seawater mass. We divided the whole ECS region into sediment and nonsediment areas. After accurately estimating the manometric sea level change, specifically the change in seawater mass, the ECS regional sea level budget could be closed within a 2-sigma uncertainty. Our results revealed that the linear trends of the regional mean sea level change in the ECS can be attributed mainly to the change in the manometric sea level (3.06 mm/year), followed by the steric component (0.44 mm/year), which contributes only ~12.57% of the total ECS regional mean sea level change rate observed via satellite altimetry. The linear trend residuals of the ECS regional sea level budget ranged from −0.12 mm/year to 0.10 mm/year, all within a 2-sigma uncertainty.

Keywords: East China Sea; sea level budget; gravity field solutions; altimetry; steric

Academic Editor: Chung-yen Kuo

Received: 9 January 2025
Revised: 26 February 2025
Accepted: 27 February 2025
Published: 1 March 2025

Citation: Wang, F.; Geng, J.; Shen, Y.; Chen, J.; Cazenave, A.; Chen, Q.; Chang, L.; Wang, W. Sea Level Budget in the East China Sea Inferred from Satellite Gravimetry, Altimetry and Steric Datasets. *Remote Sens.* **2025**, *17*, 881. https://doi.org/10.3390/rs17050881

1. Introduction

Sea level change is one of the key indicators of global climate change. With continuous global warming, the accelerated melting of polar ice sheets and mountain glaciers and the thermal expansion of the ocean have led to a steady upward trend in the global mean sea level, which has caused serious challenges in socioeconomic development and protection of the living environment, especially in coastal areas [1–3]. Since 1993, the global mean sea level has risen ~10 cm at a rate of ~3.5 mm/year according to satellite altimetry observations [4,5], which is driven mainly by manometric sea level changes related to atmosphere–ocean circulation, sea level factors and the global water cycle and steric sea level changes due to seawater density changes caused by ocean temperature and salinity variations [2,6–9]. The Gravity Recovery and Climate Experiment (GRACE)

performed satellite-based gravity measurements from 2002 to 2017 [10], and GRACE Follow-on (GRACE-FO) was successfully launched in May 2018 [11]. The GRACE/GRACE-FO monthly temporal gravity field models can be used to directly estimate global and regional land and ocean mass changes. In addition, steric sea level changes can be computed from ocean temperature and salinity observations [12,13].

Ideally, closure of the sea level budget (SLB) implies that the manometric sea level change plus steric sea level change should be close to the altimetry-based total sea level change [2,14–16]. Many previous studies have shown that the SLB can be closed at the global scale within uncertainty [6,16–18]. However, closure remains challenging at the regional scale and can only be achieved in certain regions [19–23] because regional sea level changes (e.g., in the East China Sea, ECS) can also be affected by other factors, such as continental freshwater runoff [24], estuarine sediment [25] and sea bed deformation [26], in addition to steric and manometric sea level change components [22,27]. Several previous studies have focused on ECS regional sea level variation and its possible components and drivers, such as wind stress, ocean circulation, El Niño–Southern Oscillation and other factors, using altimetry, tide gauge and steric data [28–30]. Chang and Sun [31] estimated that the ECS regional mean sea level change rate from 1993 to 2019 derived from satellite altimetry was 3.3 $\pm$ 0.2 mm/year, with 3.21 mm/year for the period from 1993 to 2021. Earlier studies revealed that steric effects accounted for approximately 40% of the observed ECS trend from 1992 to 2002 [32].

The development of various observation technologies has promoted the study of regional sea level change. Accurate identification of the causes and quantification of their contributions to total sea level change in the ECS are crucial for comprehending regional climate change. Additionally, this understanding can enhance predictions of sea level rise and its effects on coastal areas, which are vital because of their high population density [20,33]. However, few studies have focused on the ECS regional SLB. In addition to directly studying the SLB using GRACE, altimetry and steric datasets, Rietbroek et al. [19] proposed an inverse approach that combines GRACE and altimetry datasets to jointly solve for mass change and steric variations; the estimated manometric sea level change rates obtained with these methods were much lower than those obtained with the direct approach from GRACE gravity field solutions [34]. In addition, a large amount of sediment enters the ECS from major rivers, such as the Yangtze River, every year, making accurate estimation of manometric sea level changes and closing the regional SLB in the ECS challenging [35,36]. The sediment effect and seawater mass change (i.e., manometric sea level change) are normally detected by GRACE/GRACE-FO as a whole. The fundamental fact is that sediment does not contribute to sea level rise; it merely displaces the original seawater. Therefore, in theory, the sediment effect must be corrected when estimating the ECS manometric sea level change using GRACE/GRACE-FO datasets.

In this contribution, we use the latest release (version 3) of GRACE/GRACE-FO mascon solutions developed by the Jet Propulsion Laboratory (JPL) and altimetry and steric data products from April 2002 to December 2022, together with the estimated sediment discharge rates of Qiao et al. [35], to investigate the closure of ECS regional SLB directly. The remainder of this paper is structured as follows: Section 2 provides a concise overview of the study area, adopted datasets and processing methods employed in this study. Section 3 presents the results and analysis, while the discussion and conclusion are presented in Sections 4 and 5, respectively.

2. Materials, and Methods

2.1. Study Area

The East China Sea (Figure 1) is part of the western Pacific marginal sea and is localized between mainland China and Kyushu Island, the Ryukyu Islands, and Taiwan. Sea level changes in the East China Sea have a significant impact on the nearshore marine ecological environment of the southeastern coastal provinces and cities of China [37]. The long-term variations in sea level anomalies in the East China Sea are influenced by factors such as freshwater flux, sea surface wind stress, ENSO and the Kuroshio Current. The whole ECS study region (red line area) and sediment area (gray dashed area) are shown in Figure 1.

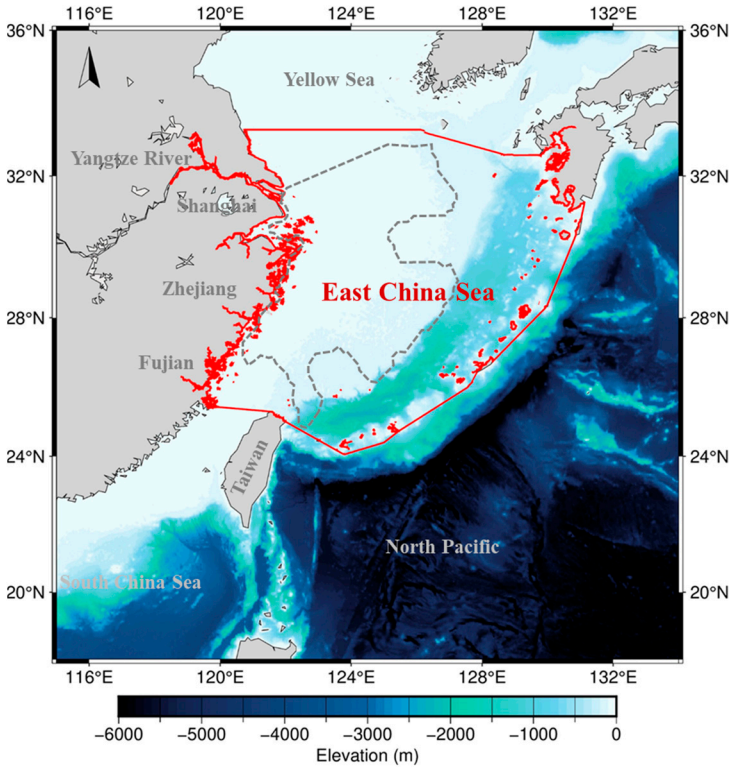

Figure 1. Whole ECS study region (red line area) and sediment area (the gray dashed area was retrieved from Qiao et al. [35]).

2.2. Adopted Datasets

2.2.1. GRACE/GRACE-FO JPL Mascon Solutions

Various groups have developed GRACE/GRACE-FO mascon solutions to increase the accuracy of observed mass changes and minimize land–ocean signal leakage [38–41]. Zhang et al. [42] evaluated different mascon solutions and reported that the Jet Propulsion Laboratory (JPL) mascon solutions perform better in estimating manometric sea level changes since they apply a coastline resolution improvement filter for reducing signal leakage [40]. Therefore, we used the GRACE/GRACE-FO JPL mascon solutions in this study. The glacial isostatic adjustment (GIA), geocentric motion (degree 1), C_{20} (degree 2, order 0) and C_{30} (degree 3, order 0) gravity coefficients in the JPL RL06 mascon solutions were all corrected. The specific details can be found in Watkins et al. [39] and Wiese et al. [40]. Notably, the GAD product, which represents gravity changes over the ocean due to nontidal atmospheric surface pressure and high-frequency oceanic mass variations, is included in the GRACE/GRACE-FO JPL RL06 mascon solutions. However, to facilitate direct comparison with satellite altimetry data, the average GAD over the ocean has been subtracted.

2.2.2. Satellite Altimetry Datasets

To estimate the regional sea level change in the East China Sea (ECS) from April 2002 to December 2022, we utilized monthly gridded merged satellite altimetry sea level anomaly products, which were developed using multiple satellite altimeter observations and distributed by the Copernicus Marine Environment Monitoring Service (CMEMS) and JPL MEaSUREs, respectively [43]. We accounted for the GIA effect in the ECS by applying the ICE6G-D GIA model [44], which involves adding a constant correction of −0.23 mm/year. Additionally, following the approaches outlined by Vishwakarma et al. [26] and Frederikse et al. [45], we subtracted the ocean bottom deformation (OBD) from the altimetry observations. The OBD can be calculated as follows [46]:

$$\Delta h(\theta, \varphi) = a \sum_{l=0}^{\infty} \sum_{m=0}^{l} \overline{p}_{lm}(\cos\theta) \frac{h_l}{1+k_l} (\Delta \overline{C}_{lm} \cos m\varphi + \Delta \overline{S}_{lm} \sin m\varphi) \quad (1)$$

where a is the average radius of the Earth; θ and φ are the colatitude and longitude, respectively; $\overline{p}_{lm}(\cos\theta)$ is the fully normalized associated Legendre function with degree l and order m; k_l and h_l are the load Love numbers of degree l within the center of the frame; and $\Delta\overline{C}_{lm}$ and $\Delta\overline{S}_{lm}$ are the spherical harmonic coefficients converted from the global mass changes in the GRACE/GRACE-FO JPL mascon solutions. According to the abovementioned postprocessing strategies, the linear trend of the OBD effects from the JPL mascon solutions is -0.25 ± 0.02 mm/year. Then, we computed the ECS regional mean total sea level changes from the two altimetry sea level anomaly grids with cosine latitude weighting and adopted the average values in the spatial and temporal domains as the final estimates.

2.2.3. Steric Observation and Reanalysis Datasets

We utilized seven publicly accessible gridded datasets containing monthly ocean temperature, salinity and pressure information to calculate the steric sea level change in the East China Sea (ECS) from April 2002 to December 2022, with an average depth of 349 m. These datasets include the global multiobservation ocean 3D temperature and salinity data (ARMOR3D) [47,48], the Institute of Atmospheric Physics (IAP) [49], EN.4.2.2 (referred to as EN4) [50] with corrections from Gouretski and Reseghetti [51] for Xpendable BathyThermograph (XBT) and from Gouretski and Cheng [52] for Mechanical BathyThermograph (MBT), the first generation of CORA released by the National Marine Data CORAV1.0 [53] covering the ocean from the surface to 2000 m depth and three reanalysis products: GLORYS version 4 (GLORYS2v4) distributed by the Copernicus Marine Environment Monitoring Service (CMEMS) [54], ocean reanalysis system 5 (ORAS5) from the European Centre for Medium-Range Weather Forecasts [55], and version 7 of the Euro-Mediterranean Center on Climate Change (CMCC) global ocean reanalysis system (C-GLORSv7) [56] extending to a 5900 m depth. Using these ocean temperature and salinity datasets, the steric sea level change can be calculated as follows [57]:

$$SL_{\text{steric}} = -\frac{1}{\rho_0} \cdot \int_{-h}^{0} \Delta\rho \cdot dz \quad (2)$$

where ρ_0 is the mean density of seawater (1.025 g/cm^3) and $\Delta\rho$ is the density change as a function of the temperature (T), salinity (S) and pressure (P). We used the spatial and temporal averages as the final estimates, and their dispersion was used to evaluate the uncertainty (Table S1).

2.2.4. Sediment Estimates

As mentioned above, sediments originating from major rivers contribute to changes in the ECS sea level. Chang et al. [36] combined GRACE, altimetry and other multisource observations to estimate that the ECS sediment change rate is 0.82 ± 0.3 Gt/year (equal to an ECS regional mean sea level change of 1.04 ± 0.4 mm/year), which is close to the estimate of Qiao et al. [35], which was independently measured from sediment cores. Therefore, to assess the consistency among the altimetry, GRACE/GRACE-FO and steric datasets, we used the estimated ECS sediment change rate provided by Qiao et al. [35] to remove the sediment effect.

2.3. Processing Methods

2.3.1. Manometric Sea Level Change Estimation Method

Similar to global SLB, the regional SLB implies that GRACE-based manometric sea level changes ($\Delta h_{\text{manometric}}$) plus steric sea level changes (Δh_{steric}) should equal the altimetry-estimated total sea level changes ($\Delta h_{\text{altimetry}}$) [2,14–16], which can be expressed as follows (Figure 1):

$$\Delta h_{\text{altimetry}} = \Delta h_{\text{steric}} + \Delta h_{\text{manometric}} + \varepsilon \tag{3}$$

where ε is the residual error.

Indeed, changes in seawater mass (referred to as the manometric sea level), sediment and the displaced original seawater mass are simultaneously observed by GRACE/GRACE-FO. Here, we represent the change in terms of the equivalent seawater height (EWH) by multiplying the thickness variation by the corresponding density.

$$\rho_{\text{sw}}\Delta h_{\text{grace}} = \rho_{\text{sw}}\Delta h_{\text{manometric}} + \rho_{\text{sed}}\Delta h_{\text{sed}} - \rho_{\text{sw}}\Delta h_{\text{sed}} \tag{4}$$

where ρ_{sw} and ρ_{sed} represent the seawater density and sediment density, respectively; Δh_{grace} represents the GRACE equivalent seawater height; and Δh_{sed} represents the sediment change.

Therefore, the seawater mass change can be derived as follows:

$$\rho_{\text{sw}}\Delta h_{\text{manometric}} = \rho_{\text{sw}}\Delta h_{\text{grace}} - \Delta h_{\text{sed}}(\rho_{\text{sed}} - \rho_{\text{sw}}) \tag{5}$$

Then, the actual manometric sea level change can be expressed as follows:

$$\Delta h_{\text{manometric}} = \Delta h_{\text{grace}} - \Delta h_{\text{sed}}(\rho_{\text{sed}}/\rho_{\text{sw}} - 1) \tag{6}$$

Note that the corrected term $\Delta h_{\text{sed}}(\rho_{\text{sed}}/\rho_{\text{sw}} - 1)$ in Equation (6) is called the "sediment effect" in this study. The seawater density (ρ_{sw}) and sediment density (ρ_{sed}) are assumed to be 1.025 g/cm^3 [35,36,58] and 1.59 g/cm^3, respectively, as suggested by Chang et al. [36].

A schematic illustration of the estimation of the actual manometric sea level change by correcting for the sediment effect in the total mass change measured by the GRACE/GRACE-FO mascon solutions and investigation of the ECS regional sea level budget is shown in Figure 2.

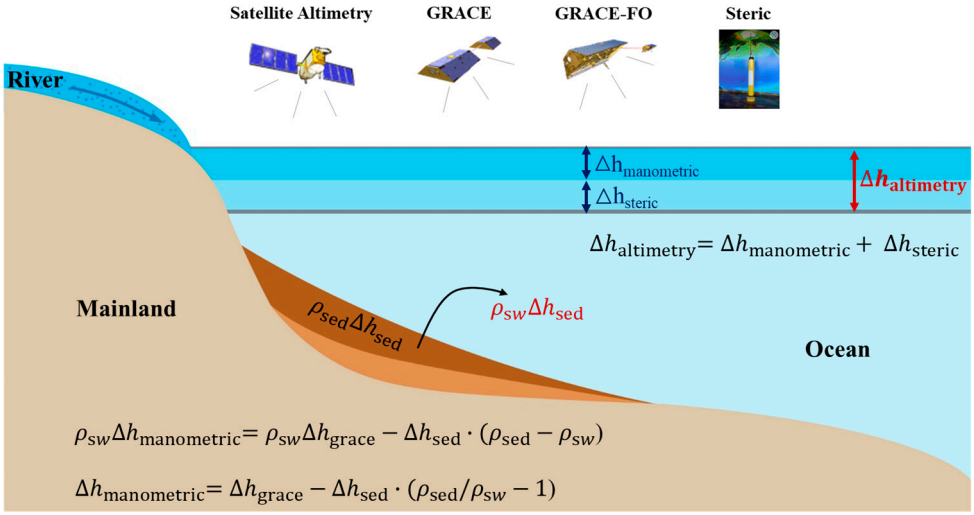

Figure 2. Regional sea level budget in the East China Sea. Note: The shadow of $\rho_{sed}\Delta h_{sed}$ represents the sediment variations.

2.3.2. Time Series Analysis

Note that all the gridded datasets utilized were resampled to a uniform grid size and a 0.25° spatial resolution, enhancing the clarity of boundary distinctions. For the ECS regional mean sea level changes derived from altimetry, steric data and GRACE/GRACE-FO JPL mascon solutions, the annual and semiannual amplitudes, as well as the linear trends, were jointly estimated using a least-squares fitting method. The associated uncertainties reflect the fitting errors, with 1 sigma for the amplitudes and phases and 2 sigma for linear trends.

3. Results and Analysis

To evaluate and quantify the contributions of the ECS SLB components to the total sea level change, in this section, we investigate the ECS sea level changes in three ECS regions, namely, the sediment area, nonsediment area and whole ECS region (Figure 1).

3.1. Temporal Analysis

From April 2002 to December 2022, the ECS regional mean sea level changes were assessed using two altimetry products: the GRACE/GRACE-FO JPL mascon solutions; and seven steric observation and reanalysis datasets, which divided the whole ECS region into sediment and nonsediment areas. The estimated regional mean sediment mass change rates based on Qiao et al. [35] in the sediment area and whole ECS region are 1.39 mm/year and 0.94 mm/year in terms of the equivalent seawater height, respectively, and 0.88 mm/year and 0.59 mm/year (i.e., the sediment replacement of original seawater), respectively, indicating that the corrected rates due to the sediment effect are 0.51 mm/year (ECS sediment area) and 0.35 mm/year (whole ECS region) and that these values should be removed from the total mass change series. Figure 3 shows the ECS regional mean total sea level changes derived from the altimetry and steric plus manometric sea level changes after correction for the sediment effect. We found that the altimetry-estimated ECS regional mean total sea level changes agreed well with those based on the steric plus manometric sea level changes for the three ECS study regions, with a high correlation coefficient (altimetry vs. steric plus manometric) of 0.97 and a root mean square error of 1.64 cm for the whole ECS region and values of 0.96 and 2.13 cm, respectively, for the sediment area and 0.97 and 1.65 cm, respectively, for the nonsediment area.

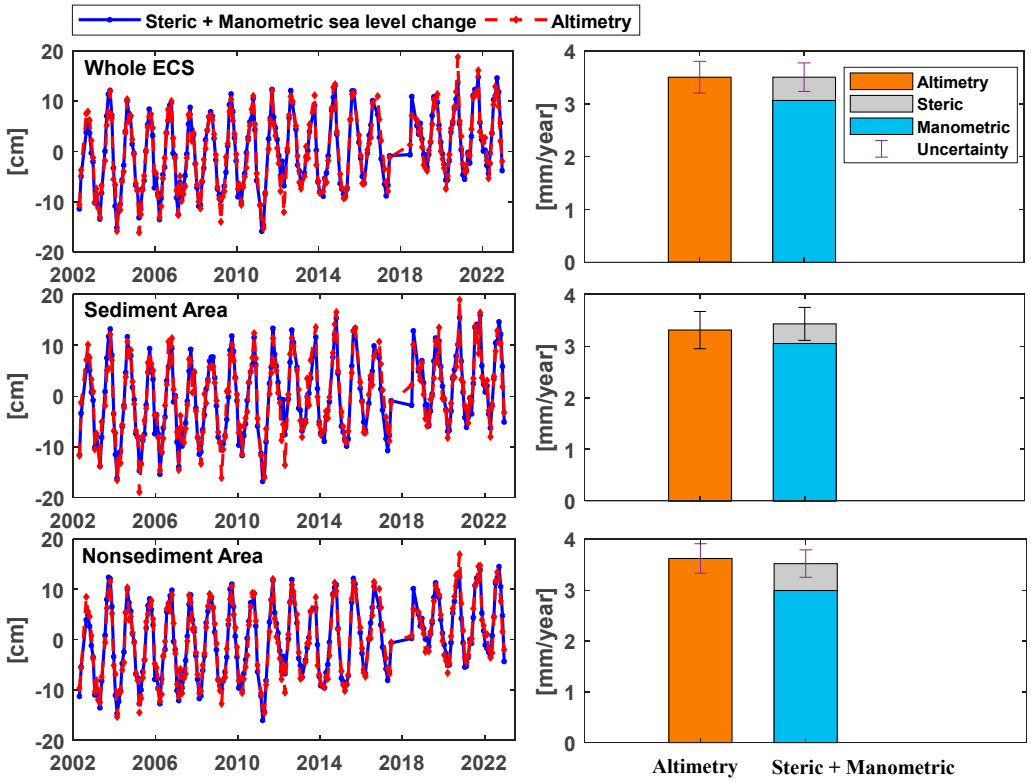

Figure 3. ECS regional mean sea level change and corresponding estimated linear trends from the altimetry, steric, GRACE/GRACE-FO JPL mascon solutions and sediment mass change estimates from Qiao et al. [36] (April 2002~December 2022).

Table 1 presents the statistical results. To ensure consistency and ease of comparison, the 33 months of missing data in the GRACE/GRACE-FO JPL mascon solutions from April 2002 to December 2022 were also removed from the altimetry and steric datasets. For the whole ECS region, the altimetry-estimated mean total sea level change rate is 3.50 ± 0.30 mm/year, which is close to that of Chang and Sun [31], with a slight difference in the studied time spans. Considering the insufficient and relatively sparse steric observations, the ECS regional mean steric sea level change rates from seven steric estimates ranged from -0.29 ± 0.12 mm/year (IAP) to 0.99 ± 0.24 mm/year (EN4), which are consistent with 0.0 ± 0.78 mm/year from Rietbroek et al. [19] and -0.05 ± 0.52 mm/year from Chang et al. [36]. The average steric sea level change rate of the seven steric estimates is 0.44 ± 0.12 mm/year, which contributed ~12.57% of the total sea level change rate from April 2002 to December 2022. The estimated rate of ECS regional total mass change is 3.41 ± 0.24 mm/year. After the sediment effect (0.35 mm/year) was removed, the manometric sea level change rate was 3.06 ± 0.24 mm/year. In fact, the sediment signal causes a -0.35 mm/year correction of the linear trend, as confirmed by Qiao et al. [35] and Chang et al. [59]. The steric plus manometric sea level change rate is 3.50 ± 0.27 mm/year, which is close to the value of 3.50 ± 0.30 mm/year inferred from satellite altimetry.

Furthermore, the annual amplitudes of regional mean steric and manometric sea level changes in the ECS are 7.65 ± 0.11 cm and 2.38 ± 0.21 cm, respectively, and the sum of these two estimates is 9.18 ± 0.24 cm, which is close to the annual amplitude of 9.24 ± 0.26 cm for total sea level change derived from satellite altimetry. This suggests that the annual variability in the total sea level change in the ECS is caused mainly by steric sea level changes. Conversely, the semiannual amplitudes are chiefly influenced by manometric sea level changes, with amplitudes of the ECS regional mean steric and manometric sea level changes of 0.09 ± 0.11 cm and 0.93 ± 0.21 cm, respectively, similar to the results estimated

in both the sediment and nonsediment study areas. Thus, we can conclude that the ECS regional sea level budget is essentially balanced in terms of linear trends, as well as annual and semiannual amplitudes and phases, for the period from April 2002 to December 2022. However, since the sediment mass change rates used are from Qiao et al. [35] without associated uncertainties, this could result in an underestimation of the uncertainty in the linear trend.

Table 1. The amplitudes of the annual and semiannual signals, as well as the linear trends, in the regional mean sea level changes obtained from altimetry, steric data and GRACE/GRACE-FO JPL mascon solutions for the period from April 2002 to December 2022.

Area	ECS Regional Mean Sea Level Change	Annual Amplitude [cm] Phase [deg]	Semiannual Amplitude [cm] Phase [deg]	Linear Trend [mm/Year]
Whole ECS	Steric	(7.65 ± 0.11) (239.2 ± 0.8)	(0.09 ± 0.11) (209.3 ± 69.4)	0.44 ± 0.12
	Total mass change	(2.38 ± 0.21) (298.1 ± 5.0)	(0.93 ± 0.21) (140.7 ± 11.6)	3.41 ± 0.24
	Sediment effect	Sediment change ($\Delta h_{sed}\rho_{sed}/\rho_{sw}$) in the form of equal seawater height; Sediment-replacement seawater changeΔh_{sed}; Sediment effect : $\Delta h_{sed}(\rho_{sed}/\rho_{sw} - 1)$		0.94/0.59/0.35
	Manometric	(2.38 ± 0.21) (298.1 ± 5.0)	(0.93 ± 0.21) (140.7 ± 11.6)	3.06 ± 0.24
	Steric plus Manometric	(9.18 ± 0.24) (253.6 ± 1.5)	(0.98 ± 0.24) (145.4 ± 13.7)	3.50 ± 0.27
	Altimetry	(9.24 ± 0.26) (256.1 ± 1.6)	(0.68 ± 0.26) (147.5 ± 21.4)	3.50 ± 0.30
Sediment	Steric	(7.99 ± 0.08) (240.7 ± 0.6)	(0.18 ± 0.08) (230.5 ± 29.5)	0.38 ± 0.09
	Total mass change	(2.99 ± 0.27) (302.5 ± 5.2)	(1.01 ± 0.27) (136.9 ± 8.2)	3.56 ± 0.31
	Sediment effect	Sediment change ($\Delta h_{sed}\rho_{sed}/\rho_{sw}$) in the form of equal seawater height; Sediment-replacement seawater changeΔh_{sed}; Sediment effect : $\Delta h_{sed}(\rho_{sed}/\rho_{sw} - 1)$		1.39/0.88/0.51
	Manometric	(2.99 ± 0.27) (302.5 ± 5.2)	(1.01 ± 0.27) (136.9 ± 8.2)	3.05 ± 0.31
	Steric plus Manometric	(9.77 ± 0.28) (256.3 ± 1.6)	(1.01 ± 0.28) (146.8 ± 15.5)	3.43 ± 0.32
	Altimetry	(9.47 ± 0.31) (256.7 ± 1.9)	(0.41 ± 0.31) (169.1 ± 43.3)	3.31 ± 0.36
Nonsediment	Steric	(7.91 ± 0.14) (241.4 ± 1.0)	(0.09 ± 0.14) (126.8 ± 92.8)	0.53 ± 0.17
	Manometric	(1.64 ± 0.17) (278.3 ± 6.0)	(0.88 ± 0.17) (131.4 ± 14.5)	2.99 ± 0.20
	Steric plus Manometric	(9.28 ± 0.23) (247.5 ± 1.4)	(0.97 ± 0.23) (131.0 ± 17.2)	3.52 ± 0.27
	Altimetry	(9.28 ± 0.25) (250.6 ± 1.5)	(0.86 ± 0.25) (120.9 ± 16.7)	3.62 ± 0.29

Note. Phase θ is defined as sin [2($t - t_0$) + θ], where t_0 refers to h_0 on 15 January. Considering that the sediment change rates used are from Qiao et al. [36] without uncertainties, here, no uncertainty is given for the rates in terms of sediment effect correction.

In a recent study, Hou et al. [60] highlighted that there has been a consistent rise in suspended sediments near global river deltas over the past two decades. In fact, the findings of this study provide evidence that correcting the sediment effect will improve the closure of regional SLBs, and one may apply the methodology to other coastal oceans that have large sediment fluxes from large rivers, such as the Amazon and Mississippi Rivers, whose annual sediment fluxes reach 1 billion tons and 100 million tons, respectively.

3.2. Spatial Analysis

In Section 3.1, we investigated the closure of the ECS regional SLB at the temporal scale. To compare the consistency among the three independent datasets in the ECS, we show the linear trend spatial distributions of the ECS SLB components in Figure 4. The linear trend distributions of the total mass change derived from the GRACE/GRACE-FO JPL mascon solutions in the ECS are shown in Figure 4a. To accurately estimate the manometric sea level change, the sediment signals need to be corrected in the total mass changes, and the corrected rates due to sedimentation changes are estimated on the basis of data measured

in situ [36], as shown in Figure 4b. After the sediment effect on the total mass change in the ECS derived from the GRACE/GRACE-FO JPL mascon solutions was corrected, the linear trend of the ECS manometric sea level change was determined, as shown in Figure 4c. While the spatial patterns of sea level change rates obtained from altimetry and the combination of steric and manometric sea level changes align in most areas, notable differences in rate magnitude and pattern persist in some regions, as shown in Figure 4e,f. In our view, these discrepancies likely stem from the uncertainties inherent in the four independent observations. These include the higher altimetry uncertainty in coastal regions, significant land–ocean signal leakage in GRACE/GRACE-FO solutions and inadequate steric data. Further investigation into these factors is necessary in future research.

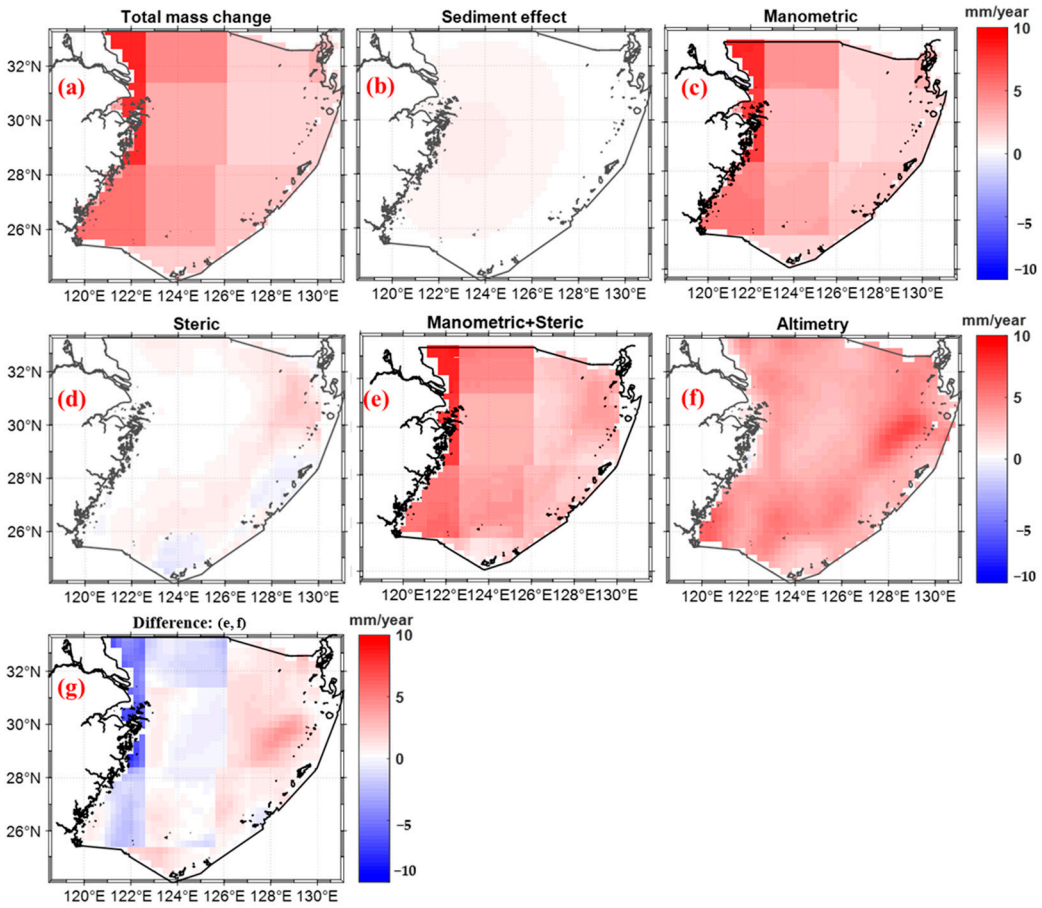

Figure 4. Linear trend distributions of regional sea level changes in the ECS. (**a**) Total mass change rate. (**b**) The estimated corrected rates due to the sediment effect based on the results of Qiao et al. [36]. (**c**) Manometric sea level change rate after removing the sediment effect. (**d**) Steric sea level change rate. (**e**) Manometric plus steric. (**f**) Altimetry-estimated ECS total sea level change rate. (**g**) Trend differences (**e**,**f**) between the altimetry (**f**) and manometric plus steric (**e**) methods.

In addition, we further show the spatial distributions in terms of annual and semiannual amplitudes in Figure 5. The results demonstrate that the annual amplitudes of manometric sea level changes are notably smaller than those of steric sea level changes. Conversely, the semiannual amplitudes exhibit the opposite relationship, a finding that aligns with the outcomes detailed in Table 1. Furthermore, the annual and semiannual amplitudes of the sum of steric and manometric sea level changes are mostly consistent with the altimetry-based estimates at the spatial scale; however, notable discrepancies between the two independent estimates do exist in certain regions, similar to the discrepancies in the linear trend distribution. Thus, it can be concluded that the annual variability in the ECS

sea level can be attributed mainly to steric effects and that manometric sea level changes contribute more to the ECS total sea level change rate and semiannual amplitude. Note that the seasonal sediment change is neglected here because only sediment mass change trends are available and used for comparison; this aspect will be further investigated in the future.

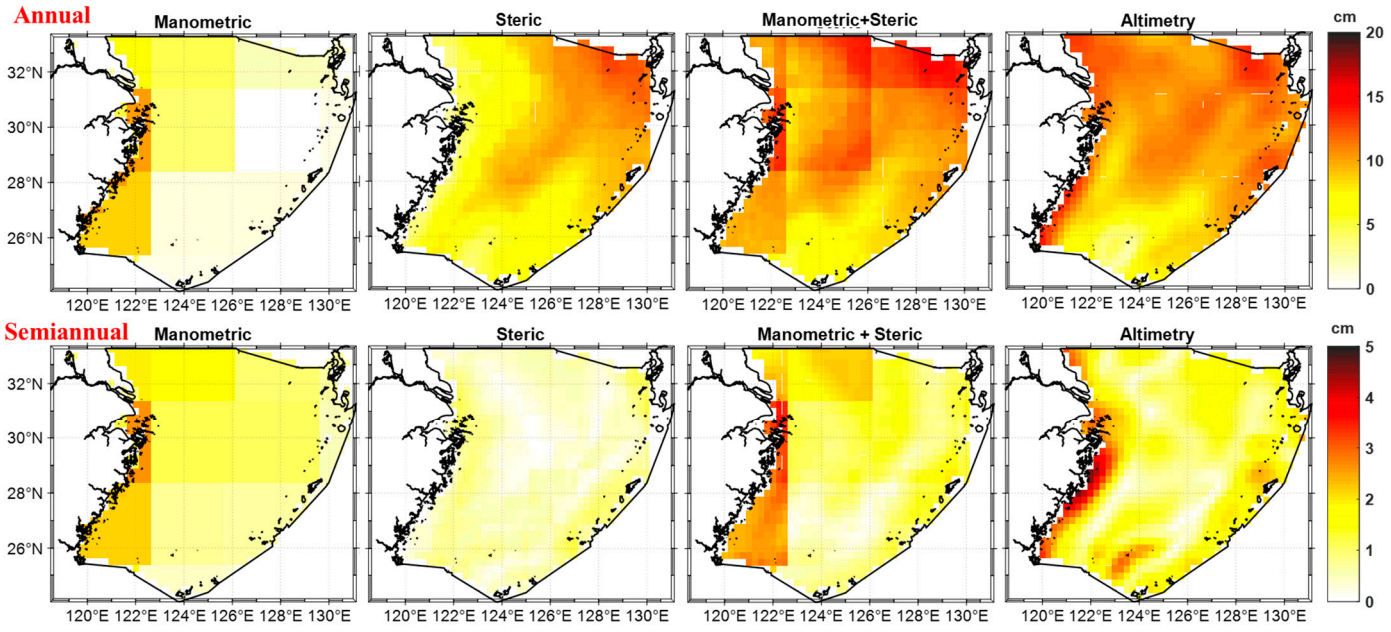

Figure 5. Annual and semiannual amplitudes of the spatial distributions of the ECS SLB components, including the manometric, steric, manometric plus steric and altimetry-based total sea level changes. Note. The seasonal variations in sediment mass change are not corrected in this part.

4. Discussions

The closure of regional sea level budgets remains a significant challenge due to the complex interplay of multiple factors influencing sea level variability. Our study successfully reconciled the ECS SLB by incorporating satellite gravimetry, altimetry, steric observations and sediment effect corrections, providing critical insights into the dominant drivers of sea level rise in this region. The findings indicate that this study provides a proof of concept that the sediment effect should be accounted for when investigating the closure of regional SLBs in coastal regions. Below, we discuss the implications of our findings, their alignment with previous studies and the remaining uncertainties that warrant further investigation.

Our results highlight that manometric sea level change (3.06 ± 0.24 mm/year) dominates the linear trend of ECS regional mean sea level rise, accounting for ~87% of the total observed rate (3.50 ± 0.30 mm/year). This aligns with global studies emphasizing ice melt and terrestrial water storage changes as primary contributors to sea level rise. However, the steric component (0.44 ± 0.12 mm/year) plays a secondary role in the ECS, contrasting with earlier regional estimates where steric effects contributed up to 40% during 1992–2002. This discrepancy may reflect decadal-scale variability in ocean heat uptake or improved observational constraints in recent datasets.

The correction for sediment effect proved critical in closing the SLB. Sediment deposition (0.94 mm/year) and its displaced seawater (0.59 mm/year) introduced a net bias of -0.35 mm/year in GRACE-derived mass trends. Neglecting this effect would have overestimated manometric contributions, underscoring the necessity of accounting for sediment dynamics in coastal regions with high fluvial sediment input, such as the ECS. This finding supports recent global assessments emphasizing sediment-induced biases in deltaic

regions. The annual amplitude of ECS regional mean sea level change is predominantly steric-driven (7.65 ± 0.11 cm), likely tied to seasonal heating/cooling cycles and monsoon-driven circulation changes. In contrast, semiannual variability is governed by manometric processes (0.93 ± 0.21 cm), potentially linked to tidal forcing or intra-annual mass redistribution. These phase-dependent contributions highlight the need to disentangle steric and mass signals when interpreting short-term sea level fluctuations.

While temporal closure was achieved, spatial mismatches persist between altimetry and steric plus manometric estimates (Figure 4). Coastal altimetry errors, GRACE signal leakage near land-ocean boundaries and sparse steric data in shallow shelves likely contribute to these discrepancies. For instance, the ECS's complex bathymetry and strong currents may amplify steric measurement uncertainties in reanalysis products. Additionally, sediment correction relied on trend-based estimates from Qiao et al. [35], which lack seasonal variability and uncertainty quantification. Incorporating transient sediment fluxes and error propagation could refine future SLB assessments.

The dominance of manometric sea level rise in the ECS suggests that ice melt and hydrological changes upstream (e.g., Yangtze River discharge) may disproportionately impact coastal vulnerability. Our methodology—correcting sediment effects—provides a template for other sediment-rich regions (e.g., Amazon Delta, Ganges–Brahmaputra). However, the relatively small steric contribution implies that thermal expansion may play a lesser role in future ECS sea level projections compared to global averages, necessitating region-specific adaptation strategies.

5. Conclusions

In this study, we investigate the ECS regional sea level budget over the period from April 2002 to December 2022 by integrating the GRACE/GRACE-FO JPL mascon solutions, two altimetry products, seven steric estimates and sediment effect corrections. The linear trend of ECS regional mean sea level rise (3.50 ± 0.30 mm/year) is primarily driven by manometric sea level change (3.06 ± 0.24 mm/year, ~87% contribution), reflecting mass redistribution from ice melt and hydrological changes. In contrast, steric effects (0.44 ± 0.12 mm/year, ~12.6% contribution) play a secondary role, contrasting with earlier regional estimates (e.g., 40% during 1992–2002), likely due to decadal variability in ocean heat uptake. The sediment deposition brought a net bias of −0.35 mm/year in GRACE-derived mass trends. Correcting this "sediment effect" was essential to closing the SLB, highlighting the necessity of accounting for sediment dynamics in coastal regions with high fluvial input, such as the Yangtze River-dominated ECS. The annual sea level fluctuations are dominated by steric effects (7.65 ± 0.11 cm amplitude), linked to thermal expansion and monsoon-driven circulation, while semiannual variability is governed by manometric processes (0.93 ± 0.21 cm amplitude), potentially tied to tidal forcing or intra-annual mass redistribution. Despite temporal closure, however, notable differences persist in certain regions between altimetry and steric plus manometric estimates, which may primarily be attributed to coastal altimetry uncertainties, GRACE signal leakage and sparse steric data in shallow shelves. Consequently, we can conclude that the ECS regional sea level budget can be closed within uncertainty. The application of the methodology to other coastal regions with large sediment fluxes from major rivers has the potential to provide a more comprehensive global perspective on the regional sea level budget.

Supplementary Materials: The following supporting information can be downloaded at https://www.mdpi.com/article/10.3390/rs17050881/s1, Table S1: The annual, semiannual amplitudes and phases, linear trends of ECS regional mean steric sea level change derived from seven steric observation and reanalysis for ECS total regions, sediment and nonsediment areas.

Author Contributions: Conceptualization, J.G., J.C. and A.C.; Methodology, F.W. and L.C.; Software, Q.C.; Validation, F.W.; Formal analysis, F.W. and Y.S.; Investigation, W.W.; Resources, Q.C. and L.C.; Writing—original draft, F.W.; Writing—review & editing, J.G., Y.S., J.C., A.C. and Q.C.; Visualization, W.W.; Supervision, J.G. and J.C.; Funding acquisition, F.W. All authors have read and agreed to the published version of the manuscript.

Funding: This work was funded by the National Natural Science Foundation of China (42374017, 42061134010 and 42394131). Professor Jianli Chen was supported by an NSFC Key Project grant (42394132).

Data Availability Statement: The GRACE/GRACE-FO JPL RL06 mascon solutions [61] can be downloaded from https://grace.jpl.nasa.gov/data/get-data/jpl_global_mascons/ accessed on 1 January 2024. The three steric ocean temperature and salinity datasets (ORAS5: [62]; GLORYS2V4: [63]; and C-GLORSv7: [64]) from the Global Ocean Ensemble Reanalysis product can be downloaded directly from https://doi.org/10.48670/moi-00024. The ARMOR3D steric dataset [65] can be downloaded from https://doi.org/10.48670/moi-00052. The three observation temperature and salinity datasets are from the websites http://www.ocean.iap.ac.cn/pages/dataService/dataService.html?navAnchor=dataService (IAP: [66]) (accessed on 20 July 2023), https://hadleyserver.metoffice.gov.uk/en4/index.html (EN.4.2.2: [67]) (accessed on 20 July 2023) and http://mds.nmdis.org.cn/pages/dataView.html?type=2&id =a5da2a0528904471b3a326c3cc85997d (CORAV1.0: [68]) (accessed on 20 July 2023). The satellite altimeter sea level anomaly datasets SEALEVEL_GLO_PHY_CLIMATE_L4_MY_008_047 [69] are available from the website https://doi.org/10.48670/moi-00148. In addition, this work used another satellite altimeter sea level anomaly dataset, SEA_SURFACE_HEIGHT_ALT_GRIDS_L4_2SATS5DAY_6THDEG_V_JPL1812 [44], which can be downloaded from the website https://doi.org/10.5067/SLREF-CDRV2. Note that for access to sediment data products, one should apply to Professor Shuqing Qiao's team at the First Institute of Oceanography under the China Ministry of Natural Resources. Detailed information about the sediment data can be found in Qiao et al. [35].

Acknowledgments: We are grateful to Shuqing Qiao and her team from the First Institute of Oceanography, China Ministry of Natural Resources, who developed the ECS sediment rates from in situ sediment data. The authors are grateful to the editor and five anonymous reviewers for their comprehensive and insightful comments, which have led to the improved presentation of the results.

Conflicts of Interest: The authors declare no conflict of interest.

References

1. Vousdoukas, M.I.; Mentaschi, L.; Voukouvalas, E.; Verlaan, M.; Jevrejeva, S.; Jackson, L.P.; Feyen, L. Global probabilistic projections of extreme sea levels show intensification of coastal flood hazard. *Nat. Commun.* **2018**, *9*, 2360. [CrossRef]
2. WCRP Sea Level Budget Group. Global sea level budget (1993–present). *Earth Syst. Sci. Data* **2018**, *10*, 1551–1590. [CrossRef]
3. Tebaldi, C.; Debeire, K.; Eyring, V.; Fischer, E.; Fyfe, J.; Friedlingstein, P.; Knutti, R.; Lowe, J.; O'Neill, B.; Sanderson, B.; et al. Climate model projections from the Scenario Model Intercomparison Project (ScenarioMIP) of CMIP6. *Earth Syst. Dyn.* **2021**, *12*, 253–293. [CrossRef]
4. Ablain, M.; Meyssignac, B.; Zawadzki, L.; Jugier, R.; Ribes, A.; Cazenave, A.; Picot, N. Error Variance-Covariance Matrix of Global Mean Sea Level Estimated from Satellite Altimetry (TOPEX, Jason 1, Jason 2, Jason 3). SEANOE. 2018. Available online: https://www.seanoe.org/data/00472/58344/ (accessed on 20 July 2023).
5. Ablain, M.; Meyssignac, B.; Zawadzki, L.; Jugier, R.; Ribes, A.; Spada, G.; Benveniste, J.; Cazenave, A.; Picot, N. Uncertainty in satellite estimates of global mean sea-level changes, trend and acceleration. *Earth Syst. Sci. Data* **2019**, *11*, 1189–1202. [CrossRef]
6. Chen, J.L.; Tapley, B.D.; Save, H.; Tamisiea, M.E.; Bettadpur, S.; Ries, J. Quantification of ocean mass change using gravity recovery and climate experiment, satellite altimeter, and Argo floats observations. *J. Geophys. Res. Solid Earth* **2018**, *123*, 10212–10225. [CrossRef]
7. Chen, Q.; Wang, F.; Shen, Y.; Zhang, X.; Nie, Y.; Chen, J. Monthly gravity field solutions from early LEO satellites' observations contribute to global ocean mass change estimates over 1993~2004. *Geophys. Res. Lett.* **2022**, *49*, e2022GL099917. [CrossRef]
8. Jeon, T.; Seo, K.-W.; Youm, K.; Chen, J.L.; Wilson, C.R. Global sea level change signatures observed by GRACE satellite gravimetry. *Sci. Rep.* **2018**, *8*, 13519. [CrossRef] [PubMed]

9. Wang, F.; Shen, Y.; Chen, Q.; Chen, J.; Geng, J. Global Sea Level Change Rate, Acceleration and Its Components from 1993 to 2016. *Mar. Geodesy* **2023**, *47*, 23–40. [CrossRef]
10. Tapley, B.; Bettadpur, S.; Ries, J.; Thompson, P.; Watkins, M. GRACE measurements of mass variability in the Earth system. *Science* **2004**, *305*, 503–505. [CrossRef]
11. Landerer, F.; Flechtner, F.; Save, H.; Webb, F.H.; Bandikova, T.; Bertiger, W.I.; Bettadpur, S.V.; Byun, S.H.; Dahle, C.; Dobslaw, H.; et al. Extending the global mass change data record: GRACE Follow-On instrument and science data performance. *Geophys. Res. Lett.* **2020**, *47*, e2020GL088306. [CrossRef]
12. Levitus, S.; Antonov, J.; Boyer, T. Warming of the world ocean. *Geophys. Res. Lett.* **2005**, *32*, 1955–2003. [CrossRef]
13. Ishii, M.; Kimoto, M.; Sakamoto, K.; Iwasaki, S.-I. Steric sea level changes estimated from historical ocean subsurface temperature and salinity analyses. *J. Oceanogr.* **2006**, *62*, 155–170. [CrossRef]
14. Dieng, H.B.; Cazenave, A.; von Schuckmann, K.; Ablain, M.; Meyssignac, B. Sea level budget over 2005–2013: Missing contributions and data errors. *Ocean Sci.* **2015**, *11*, 789–802. [CrossRef]
15. Chambers, D.P.; Cazenave, A.; Champollion, N.; Dieng, H.; Llovel, W.; Forsberg, R.; von Schuckmann, K.; Wada, Y. Evaluation of the global mean sea level budget between 1993 and 2014. *Surv. Geophys.* **2016**, *38*, 309–327. [CrossRef]
16. Wang, F.; Shen, Y.; Chen, Q. Reduced Misclosure of Global Sea-Level Budget Using New Released Tongji-Grace2018 Solution. *Sci. Rep.* **2021**, *11*, 17667. [CrossRef]
17. Cazenave, A.; Dominh, K.; Guinehut, S.; Berthier, E.; Llovel, W.; Ramillien, G.; Ablain, M.; Larnicol, G. Sea level budget over 2003–2008: A reevaluation from GRACE space gravimetry, satellite altimetry and Argo. *Glob. Planet. Change* **2009**, *65*, 83–88. [CrossRef]
18. Frederikse, T.; Landerer, F.; Caron, L.; Adhikari, S.; Parkes, D.; Humphrey, V.W.; Dangendorf, S.; Hogarth, P.; Zanna, L.; Cheng, L. The causes of sea-level rise since 1900. *Nature* **2020**, *584*, 393–397. [CrossRef]
19. Rietbroek, R.; Brunnabend, S.-E.; Kusche, J.; Schröter, J.; Dahle, C. Revisiting the contemporary sea-level budget on global and regional scales. *Proc. Natl. Acad. Sci. USA* **2016**, *113*, 1504–1509. [CrossRef]
20. Royston, S.; Vishwakarma, B.D.; Westaway, R.; Rougier, J.; Sha, Z.; Bamber, J. Can we resolve the basin-scale sea level trend budget from GRACE ocean mass? *J. Geophys. Res.* **2020**, *125*, e2019JC015535. [CrossRef]
21. Yang, Y.; Feng, W.; Zhong, M.; Mu, D.; Yao, Y. Basin-Scale Sea Level Budget from Satellite Altimetry, Satellite Gravimetry, and Argo Data over 2005 to 2019. *Remote Sens.* **2022**, *14*, 4637. [CrossRef]
22. Camargo, C.M.L.; Riva, R.E.M.; Hermans, T.H.J.; Marcos, M.; Schütt, E.M.; Hernandez-Carrasco, I.; Slangen, A.B.A. Regionalizing the Sea-level Budget with Machine Learning Techniques. *Ocean Sci.* **2023**, *19*, 17–41. [CrossRef]
23. Ludwigsen, C.B.; Andersen, O.B.; Marzeion, B.; Malles, J.-H.; Schmied, H.M.; Döll, P.; Watson, C.; King, M.A. Global and regional ocean mass budget closure since 2003. *Nat. Commun.* **2024**, *15*, 1416. [CrossRef]
24. Durand, F.; Piecuch, C.G.; Becker, M.; Papa, F.; Raju, S.V.; Khan, J.U.; Ponte, R.M. Impact of Continental Freshwater Runoff on Coastal Sea Level. *Surv. Geophys.* **2019**, *40*, 1437–1466. [CrossRef]
25. Mouyen, M.; Longuevergne, L.; Steer, P.; Crave, A.; Lemoine, J.-M.; Save, H.; Robin, C. Assessing modern river sediment discharge to the ocean using satellite gravimetry. *Nat. Commun.* **2018**, *9*, 3384. [CrossRef] [PubMed]
26. Vishwakarma, B.D.; Royston, S.; Riva, R.; Westaway, R.M.; Bamber, J.L. Sea level budgets should account for ocean bottom deformation. *Geophys. Res. Lett.* **2019**, *47*, e2019GL086492. [CrossRef]
27. Gregory, J.M.; Griffies, S.M.; Hughes, C.W.; Lowe, J.A.; Church, J.A.; Fukimori, I.; Gomez, N.; Kopp, R.E.; Landerer, F.; Cozannet, G.L.; et al. Concepts and Terminology for Sea Level: Mean, Variability and Change, Both Local and Global. *Surv. Geophys.* **2019**, *40*, 1251–1289. [CrossRef]
28. Yan, M.; Zuo, J.-C.; Du, L.; Li, L.; Li, P.-L. Sea Level Variation/Change and Steric Contributions in the East China Sea. In Proceedings of the 17th International Offshore and Polar Engineering Conference, Lisbon, Portugal, 1–6 July 2007; pp. 2377–2382.
29. Qiao, X.; Chen, G. A Preliminary Analysis on the China Sea Level Using 11 Years' TOPEX/Poseidon Altimeter Data. *Mar. Sci.* **2008**, *32*, 60–64.
30. Zhang, S.; Du, L.; Chang, Y.; Li, J. Interannual and Decadal Variation of Sea Level in the East China Sea. In Proceedings of the 22nd International Offshore and Polar Engineering Conference (ISOPE2012), Rhodes, Greece, 17–22 June 2012; Volume 3, pp. 693–700.
31. Chang, L.; Sun, W.K. Progress and prospect of sea level changes of global and China nearby seas. *Rev. Geophys. Planet. Phys.* **2021**, *52*, 266–279.
32. Han, G.; Huang, W. Pacific Decadal Oscillation and sea level variability in the Bohai, Yellow and ECSS. *Phys. Oceanogr.* **2008**, *38*, 2772–2783. [CrossRef]
33. Kleinherenbrink, M.; Riva, R.; Sun, Y. Sub-basin-scale sea level budgets from satellite altimetry, Argo floats and satellite gravimetry: A case study in the North Atlantic Ocean. *Ocean Sci.* **2016**, *12*, 1179–1203. [CrossRef]
34. Uebbing, B.; Kusche, J.; Rietbroek, R.; Landerer, F.W. Processing choices affect ocean mass estimates from GRACE. *J. Geophys. Res. Ocean* **2019**, *124*, 1029–1044. [CrossRef]

35. Qiao, S.; Shi, X.; Wang, G.; Zhou, L.; Hu, B.; Hu, L.; Yang, G.; Liu, Y.; Yao, Z.; Liu, S. Sediment accumulation and budget in the Bohai Sea, Yellow Sea and East China Sea. *Mar. Geol.* **2017**, *390*, 270–281. [CrossRef]
36. Chang, L.; Tang, H.; Yi, S.; Sun, W. The trend and seasonal change of sediment in the East China Sea detected by GRACE. *Geophys. Res. Lett.* **2019**, *46*, 1250–1258. [CrossRef]
37. Wang, G.; Kang, J.; Yan, G.; Han, G.; Han, Q. Spatio-temporal variability., sea level in the East China Sea. *J. Coast. Res.* **2015**, *73*, 40–47. [CrossRef]
38. Save, H. *CSR GRACE and GRACE-FO RL06 Mascon Solutions v02*; University of Texas: Austin, TX, USA, 2020. [CrossRef]
39. Watkins, M.M.; Wiese, D.N.; Yuan, D.-N.; Boening, C.; Landerer, F.W. Improved methods for observing Earth's time variable mass distribution with GRACE using spherical cap mascons. *J. Geophys. Res. Solid Earth* **2015**, *120*, 2648–2671. [CrossRef]
40. Wiese, D.N.; Landerer, F.W.; Watkins, M.M. Quantifying and reducing leakage errors in the JPL RL05M GRACE Mascon solution. *Water Resour. Res.* **2016**, *52*, 7490–7502. [CrossRef]
41. Loomis, B.D.; Luthcke, S.B.; Sabaka, T.J. Regularization and error characterization of GRACE mascons. *J. Geodesy* **2019**, *93*, 1381–1398. [CrossRef]
42. Zhang, L.; Sun, W.K. Progress and prospect of GRACE Mascon product and its application. *Rev. Geophys. Planet. Phys.* **2021**, *52*, 35–52.
43. Peltier, R.; Argus, D.; Drummond, R. Comment on "an assessment of the ICE-6G_C (VM5a) glacial isostatic adjustment model" by Purcell et al. *J. Geophys. Res. Solid Earth* **2018**, *123*, 2019–2028. [CrossRef]
44. Zlotnicki, V.; Qu, Z.; Willis, J. SEA_SURFACE_HEIGHT_ALT_GRIDS_L4_ 2SATS_5DAY_6THDEG_V_JPL1609. Ver. 1812. PO.DAAC, CA, USA. 2019. Available online: https://podaac.jpl.nasa.gov/dataset/SEA_SURFACE_HEIGHT_ALT_GRIDS_L4_2SATS_5DAY_6THDEG_V_JPL1812 (accessed on 20 July 2023). [CrossRef]
45. Frederikse, T.; Riva, R.; King, M.A. Ocean bottom deformation due to present-day mass redistribution and its impact on sea level observations. *Geophys. Res. Lett.* **2017**, *44*, 12–306. [CrossRef]
46. van Dam, T.; Wahr, J.; Lavallée, D. A comparison of annual vertical crustal displacements from GPS and Gravity Recovery and Climate Experiment (GRACE) over Europe. *J. Geophys. Res.* **2007**, *112*, B03404. [CrossRef]
47. Guinehut, S.; Dhomps, A.-L.; Larnicol, G.; Le Traon, P.-Y. High resolution 3D temperature and salinity fields derived from in situ and satellite observations. *Ocean Sci.* **2012**, *8*, 845–857. [CrossRef]
48. Mulet, S.; Rio, M.H.; Mignot, A.; Guinehut, S.; Morrow, R. A new estimate of the global 3D geostrophic ocean circulation based on satellite data and in-situ measurements. *Deep. Sea Res. Part II Top. Stud. Oceanogr.* **2012**, *77*, 70–81. [CrossRef]
49. Li, G.; Cheng, L.; Pan, Y.; Wang, G.; Liu, H.; Zhu, J.; Zhang, B.; Ren, H.; Wang, X. A global gridded ocean salinity dataset with 0.5 horizontal resolution since 1960 for the upper 2000 m. *Front. Mar. Sci.* **2023**, *10*, 1108919. [CrossRef]
50. Good, A.; Martin, M.J.; Rayner, N.A. EN4: Quality controlled ocean temperature and salinity profiles and monthly objective analyses with uncertainty estimates. *J. Geophys. Res. Ocean.* **2013**, *118*, 6704–6716. [CrossRef]
51. Gouretski, V.; Reseghetti, F. On depth and temperature biases in bathythermograph data: Development of a new correction scheme based on analysis of a global ocean database. *Deep Sea Res. Part I Oceanogr. Res. Pap.* **2010**, *57*, 812–833. [CrossRef]
52. Gouretski, V.; Cheng, L. Correction for Systematic Errors in the Global Dataset of Temperature Profiles from Mechanical Bathythermographs. *J. Atmos. Technol. Ocean. Res.* **2020**, *37*, 5. [CrossRef]
53. Fu, H.; Dan, B.; Gao, Z.; Wu, X.; Chao, G.; Zhang, L.; Zhang, Y.; Liu, K.; Zhang, X.; Li, W. Global ocean reanalysis CORA2 and its inter comparison with a set of other reanalysis products. *Front. Mar. Sci.* **2023**, *10*, 1084186. [CrossRef]
54. Verezemskaya, P.; Barnier, B.; Gulev, S.K.; Gladyshev, S.; Molines, J.; Gladyshev, V.; Lellouche, J.; Gavrikov, A. Assessing eddying (1/12°) ocean reanalysis GLORYS12 using the 14-yr instrumental record from 59.5° N section in the Atlantic. *J. Geophys. Res.-Oceans* **2021**, *126*, e2020JC016317. [CrossRef]
55. Zuo, H.; Balmaseda, M.A.; Tietsche, S.; Mogensen, K.; Mayer, M. The ECMWF operational ensemble reanalysis-analysis system for ocean and sea ice: A description of the system and assessment. *Ocean Sci.* **2019**, *15*, 779–808. [CrossRef]
56. Storto, A.; Masina, S. C-GLORSv5: An improved multipurpose global ocean eddy-permitting physical reanalysis. *Earth Syst. Sci. Data* **2016**, *8*, 679–696. [CrossRef]
57. Chen, J.L.; Wilson, C.R.; Tapley, B.D.; Hu, X.G. Thermosteric effects on interannual and long-term global mean sea level changes. *J. Geodesy* **2006**, *80*, 240–247. [CrossRef]
58. Liu, Y.; Hwang, C.; Han, J.; Kao, R.; Wu, C.-R.; Shih, H.-C.; Tangdamrongsub, N. Sediment-Mass accumulation rate and variability in the East China Sea detected by GRACE. *Remote Sens.* **2016**, *8*, 777. [CrossRef]
59. Chang, L.; Qian, A.; Yi, S.; Xu, C.; Sun, W. Sea level change in China adjacent seas studied using satellite altimeter, satellite gravity, and thermohaline data. *J. Univ. Chin. Acad. Sci.* **2017**, *34*, 371–379.
60. Hou, X.; Xie, D.; Feng, L.; Shen, F.; Nienhuis, J.H. Sustained increase in suspended sediments near global river deltas over the past two decades. *Nat. Commun.* **2024**, *15*, 3319. [CrossRef]

61. Wiese, D.; Yuan, D.; Boening, C.; Landerer, F.W.; Watkins, M.M. JPL GRACE Mascon Ocean, Ice, and Hydrology Equivalent Water Height Release 06 Coastal Resolution Improvement (CRI) Filtered Version 1.0. Ver. 1.0. PO.DAAC, CA, USA [Dataset]. 2018. Available online: https://podaac.jpl.nasa.gov/dataset/TELLUS_GRACE_MASCON_CRI_GRID_RL06_V1# (accessed on 24 August 2023). [CrossRef]
62. Zuo, H.; Balmaseda, M.A.; Tietsche, S.; Mogensen, K.; Mayer, M. Global Ocean Ensemble Reanalysis Product. E.U. Copernicus Marine Service Information (CMEMS). Marine Data Store (MDS). [Dataset]. 2023. Available online: https://data.marine.copernicus.eu/product/GLOBAL_MULTIYEAR_PHY_ENS_001_031/description (accessed on 4 July 2023). [CrossRef]
63. Verezemskaya, P.; Barnier, B.; Gulev, S.K.; Gladyshev, S.; Molines, J.; Gladyshev, V.; Lellouche, J.; Gavrikov, A. Global Ocean Ensemble Reanalysis Product. E.U. Copernicus Marine Service Information (CMEMS). Marine Data Store (MDS). [Dataset]. 2023. Available online: https://data.marine.copernicus.eu/product/GLOBAL_MULTIYEAR_PHY_ENS_001_031/description (accessed on 4 July 2023). [CrossRef]
64. Global Ocean Ensemble Reanalysis Product. E.U. Copernicus Marine Service Information (CMEMS). Marine Data Store (MDS). [Dataset]. Available online: https://data.marine.copernicus.eu/product/GLOBAL_MULTIYEAR_PHY_ENS_001_031/description (accessed on 20 July 2023). [CrossRef]
65. Guinehut, S.; Dhomps, A.-L.; Larnicol, G.; Le Traon, P.-Y. Multi Observation Global Ocean 3D Temperature Salinity Height Geostrophic Current and MLD. E.U. Copernicus Marine Service Information (CMEMS). Marine Data Store (MDS). [Dataset]. 2023. Available online: https://data.marine.copernicus.eu/product/MULTIOBS_GLO_PHY_TSUV_3D_MYNRT_015_012/description (accessed on 4 July 2023). [CrossRef]
66. Li, G.; Cheng, L.; Pan, Y.; Wang, G.; Liu, H.; Zhu, J.; Zhang, B.; Ren, H.; Wang, X. IAP Global Ocean Temperature and Salinity 0.5° Gridded Dataset. 2023. Available online: http://www.ocean.iap.ac.cn/pages/dataService/dataService.html?navAnchor=dataService (accessed on 20 July 2023).
67. Good, A.; Martin, M.J.; Rayner, N.A. EN.4.2.2. 2024. Available online: https://www.metoffice.gov.uk/hadobs/en4/ (accessed on 20 July 2023).
68. Fu, H.; Dan, B.; Gao, Z.; Wu, X.; Chao, G.; Zhang, L.; Zhang, Y.; Liu, K.; Zhang, X.; Li, W. Global ocean reanalysis CORA2 and its inter comparison with a set of other reanalysis products. [Dataset]. 2023. Available online: http://mds.nmdis.org.cn/pages/dataView.html?type=2&id=a5da2a0528904471b3a326c3cc85997d. (accessed on 20 July 2023).
69. CMEMS (Copernicus Marine Service Information). Global Ocean Gridded L4 Sea Surface Heights and Derived Variables Reprocessed Copernicus Climate Service. Marine Data Store (MDS). 2023. Available online: https://data.marine.copernicus.eu/product/SEALEVEL_GLO_PHY_CLIMATE_L4_MY_008_057/description (accessed on 4 July 2023). [CrossRef]